Numerical modelling of concrete-filled aluminium alloy 6082-T6 columns under axial compression

Numerical modelling of concrete-filled aluminium alloy 6082-T6 columns under axial compression

Evangelia Georgantzia, Shafayat Bin Ali, Michaela Gkantou[1], George S Kamaris, Patryk Kot and Khalid Hashim

School of Civil Engineering and Built Environment, Faculty of Engineering and Technology, Liverpool John Moores University, Liverpool L3 3AF, UK

Abstract. Aluminium alloys are characterised by numerous benefits, such as ease of fabrication, good strength-to-weight ratio, attractive appearance and high corrosion resistance. On the other hand, aluminium has low Young's Modulus and as a result, it is susceptible to structural instability phenomena that can subsequently affect the structural integrity. Improved strength and stiffness can be achieved by combining aluminium alloys with concrete. The present work investigates numerically the response of concrete-filled aluminium tubular members under axial compression. In particular, 6082-T6 extruded aluminium alloy rectangular and square hollow sections filled with C30 concrete are examined. Finite element models are developed accounting for geometric and material non-linearities. Upon validation against experimental data, the finite element models are used to conduct a thorough parametric study over a wide range of structural members likely to occur in practice to investigate their structural behaviour under axial compression. The obtained load capacities are discussed and remarks on the structural response and on the buckling behaviour are reported. Design recommendations for the buckling strength of concrete-filled aluminium tubular columns on the basis of the numerical analyses are also made.

Keywords. aluminium alloys, concrete-filled tubes, numerical analysis, buckling behaviour, structural design, composite structures

1. Introduction

Over the last years there is an increased application of aluminium alloys as structural material owing to their advantages [1]. In particular, 25% of the overall aluminium production is on the construction industry. Aluminium alloys are characterised by high strength-to-weight ratio, ease of extrusion, considerable ductility, attractive appearance and high corrosion resistance. Despite these profound benefits, aluminium alloys have Young's Modulus of only 70 MPa resulting in lower stiffness and load-carrying capacity compared to conventional metallic structural materials such as carbon steel. Nonetheless, this downside could be counterbalanced by aluminium alloys with concrete, one of the most frequent construction materials. Combining these two materials, high stiffness and strength could be achieved, thereby reducing their sensitivity to instability phenomena. On this direction, Zhou and Young [2,3] studied experimentally and numerically the performance of concrete-filled aluminium tubular (CFAT) short columns and suggested relevant structural design framework [4]. Moreover, Zhou

[1] Corresponding author.
E-mail address: M.Gkantou@ljmu.ac.uk

and Young [5] investigated another cross-sectional type, i.e. double-skin aluminium tubes, infilled with concrete under axial compression and proposed design strength formulae. Given that only limited studies on the combination of these two structural materials have been reported, further investigation is needed.

Aiming for a better comprehension of the structural performance of composite aluminium-concrete structures, this paper presents a study on CFAT by finite element (FE) modelling. Last decades, FE techniques have been widely used as an effective tool for design and research problems in various engineering fields and hence in structural engineering. The degree of accuracy of a FE model is dependent on different parameters such as the material modelling, the boundary conditions, the interaction between surfaces in contact and so on. For this reason, the accuracy of the numerical models should be evaluated on the basis of experimental data [6-9]. Using the commercially available FE package ABAQUS [10], this paper presents the numerical investigation of CFAT columns. The interaction properties between the concrete infill and the aluminium tube and material modelling of concrete were carefully considered. The obtained numerical results were verified against the experimental ones reported by [11]. A parametric study was carried out considering a wide variety of parameters such as the cross-sectional aspect ratio (*h/b*), slenderness and concrete strength. Finally, the column strengths predicted by the FE models were used to assess the European design standards [12,13].

2. FE model

2.1. Overview of the models

A FE model capable of capturing accurately the buckling response of CFAT members was initially developed. The model aimed to simulate the non-linear behaviour of aluminium alloy square (SHS) and rectangular hollow sections (RHS), filled with concrete and subjected to gradually increased axial compressive loading. Recent experimental investigations on CFAT columns under axial compression performed by Georgantzia et al. [11] were used to validate the FE model developed in this numerical study. In [11], a total of 10 members with pin-ended support conditions were tested. The specimens comprised RHS and SHS and were fabricated by extrusion of 6082-T6 heat treated aluminium alloy. Various cross-sections aspect ratios (*h/b*) were considered. The aluminium tubes were filled with concrete of C30 grade and had length equal to 1 m. Prior to the testing, tensile tests on aluminium alloy coupons have been executed to obtain the material properties. All specimens failed due to flexural buckling around the minor axis. The measured material properties and dimensions of the specimens in [11] are summarised for reference in table 1, where E_a, f_y and f_{ck} are the Young's Modulus of aluminium, the proof strength of aluminium and the compressive strength of concrete, respectively. The FE models developed in the first part of this study replicate the 10 specimens reported in [11]. This section discusses key numerical modelling parameters such as element type and mesh, applied boundary conditions, initial geometric imperfections, material modelling and load application that will allow a successful validation of the FE model.

Table 1. Summary of the test program [11].

Specimen	Height, *h* (mm)	Width, *b* (mm)	*h/b*	Thickness, *t* (mm)	Length, *L* (mm)	E_a (MPa)	f_y (MPa)	f_{ck} (MPa)
S50.8×50.8×1.6	50.70	51.02	1.00	1.61	1001.0	65.0	289.1	31.57
S50.8×50.8×3.3	50.64	50.60	1.00	3.13	1000.6	71.7	302.2	31.57
S50.8×50.8×4.8	50.63	50.60	1.00	4.67	999.9	67.5	305.9	31.57
S76.2×76.2×3.3	76.36	76.36	1.00	3.23	1000.9	66.2	299.1	31.57
S76.2×76.2×4.8	76.18	76.14	1.00	4.76	1001.0	64.7	306.1	31.57
S76.2×76.2×6.4	76.32	76.29	1.00	6.28	1000.8	69.3	295.3	31.57
R76.2×38.1×3.3	76.21	38.20	1.99	3.27	1001.0	68.5	276.8	31.57
R76.2×47.8×3.3	76.11	50.74	1.53	3.18	1000.5	67.5	289.5	31.57
R101.6×25.4×3.3	101.81	25.40	3.99	3.22	1000.2	63.9	242.5	31.57
R101.6×50.8×3.3	101.84	51.42	1.98	3.42	1000.6	60.0	183.8	31.57

2.2. Element type and mesh

Various elements are available for the development of finite element models and the choice is dependent on the application. The eight-node brick elements with three translational degrees of freedom at each node and reduced integration (C3D8R) were chosen to simulate the aluminium tube and the concrete infill, allowing for reasonable computational times. An initial mesh convergence study was carried out to define the optimal mesh size which allows for high accuracy at lowest possible computational cost. A structured mesh with element size equal to the thickness of the aluminium tube was considered, while three elements through the thickness of the aluminium tube were employed. A typical specimen was discretised in 60000 elements.

2.3 Boundary conditions

Due to symmetry in boundary conditions, load application, geometry and buckling modes shape, only half of the section was modelled saving computational time without compromising accuracy. The applied boundary conditions aimed to replicate those of [11], i.e. pin-ended support conditions enabling rotation along one axis. Figure 1 shows a typical model along with the applied boundary conditions. Kinematic coupling constraints were used to simulate the end boundary conditions. All three translational degrees of freedom (DOFs) were restrained at both ends, except from the longitudinal translation at the top loaded end. The rotational DOFs were restrained for both ends except of the examined rotation axis that was kept free at both ends.

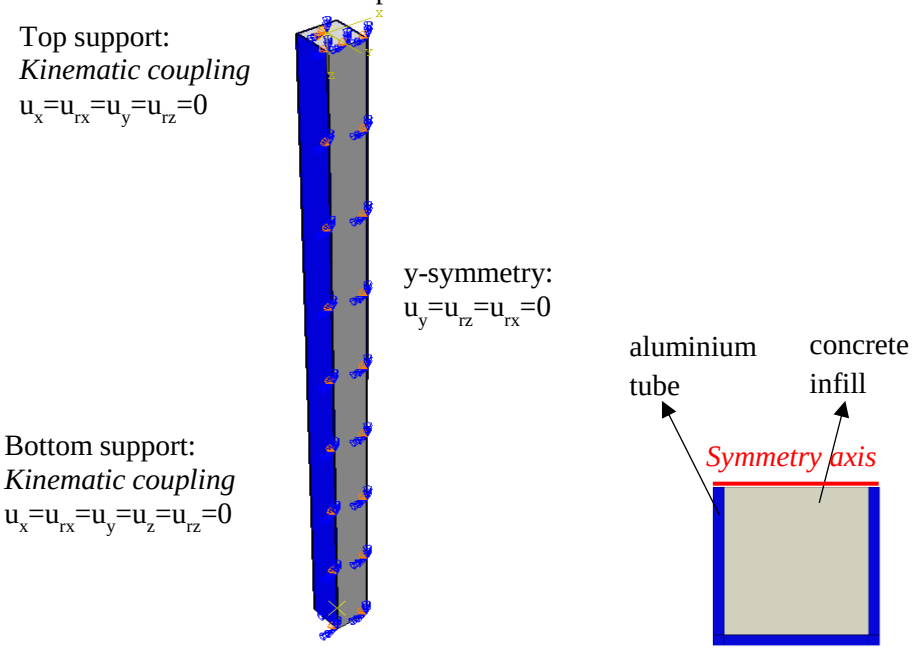

Figure 1. Geometrical modelling and applied boundary conditions.

2.4. Material modelling of aluminium tubes

Aluminium alloys exhibit a rounded stress-strain relationship and herein the engineering stress-strain curves of 6082-T6 reported in [11] were adopted. The initial elastic part was described using the Poisson's ratio (v), which was defined equal to 0.33 and isotropic hardening behaviour was adopted. The analytical equations (1) and (2) were used to convert the engineering stress and strain values to true stress and logarithmic plastic strain values respectively.

$$\sigma_{true} = \sigma_{engineering}(1+\varepsilon_{engineering}) \quad (1)$$

$$\varepsilon_{\ln}^{pl} = \ln(1+\varepsilon_{engineering}) - \frac{\sigma_{true}}{E_a} \tag{2}$$

where σ_{true} is the true stress, $\sigma_{engineering}$ is the measured stress, $\varepsilon_{engineering}$ is the measured strain, $\varepsilon^{pl}{}_{ln}$ is the logarithmic plastic strain and E_a is the Young's Modulus of aluminium tubes.

2.5. Material modelling of concrete infill

In line with past studies [9, 14-16], the concrete damage plasticity model was used in the current investigation. This model can effectively capture the behaviour of concrete in the plastic range by adopting a Drucker-Prager hyperbolic flow potential function. Since the specimens underwent monotonic loading it is not necessary for damage variables to be defined. The key material parameters comprise the dilation angle (ψ), the viscosity parameter, the flow potential eccentricity (e), the ratio of the compressive strength under biaxial loading over the uniaxial compressive strength (f_{b0}/f'_c), the ratio of the second stress invariant on the tensile meridian over that on the compressive meridian (K_c), the Young's Modulus (E_c), the tensile behaviour and strain hardening/softening rule.

In the current model, default values of 0.1 and 0 were taken for e and the viscosity parameter, respectively [9]. Tao et al. [9] suggested that a constant value of ψ=40° provides the best approximation of the ultimate strength of concrete-filled steel tubular short columns and hence this value was adopted herein. In addition, the Poisson's ratio (v) is defined equal to 0.2. Empirical equation (3) recommended in European standards for the structural design of concrete (EC2) [17] is used to define E_c:

$$E_c = 22000\left(\frac{f'_c+8}{10}\right)^{0.3} \tag{3}$$

where f'_c is the compressive cylinder strength in MPa.

The f_{b0}/f'_c ratio is estimated according to equation (4) proposed by Papanikolaou and Kappos [18]:

$$\frac{f_{b0}}{f'_c} = 1.5\left(f'_c\right)^{-0.075} \tag{4}$$

K_c is a fundamental parameter for defining the yield surface in concrete damage plasticity model [9]. Equation (5) suggested by Yu et al. [19] was employed herein to calculate K_c:

$$K_c = \frac{5.5 f_{b0}}{3 f'_c + 5 f_{b0}} \tag{5}$$

The tensile behaviour was set to be linear until $0.1 f'_c$ which taken as the maximum uniaxial tensile strength of concrete. Beyond this point, the failure mechanism is characterised by softening behaviour which can be described adequately by Hillerborg's [20] fracture energy cracking model. According to this model, the fracture energy, G_F, is the required energy to open a unit area of crack and can be treated as material parameter using brittle fracture concepts. In this study, the stress-crack opening displacement from equations (6)-(7), developed by Hordijk [21] were adopted:

$$\frac{\sigma_t}{f_t} = \left\{\left[1+\left(c_1\frac{w_t}{w_{cr}}\right)^3\right]\exp\left(-c_2\frac{w_t}{w_{cr}}\right)\right\} - \frac{w_t}{w_{cr}}\left(1+c_1^3\right)\exp\left(-c_2\right) \tag{6}$$

$$w_{cr} = 5.14\frac{G_F}{f_t} \tag{7}$$

where w_t is the crack opening displacement, w_{cr} is the crack opening displacement corresponding to the complete loss of tensile strength, σ_t is the tensile stress normal to the direction of the crack, f_t is the uniaxial tensile strength of concrete and c_1 and c_2 constants equal to 3 and 6.93 respectively. The G_F is estimated according to equation (8) [22,23]:

$$G_F = \left(0.0469 d_a^2 - 0.5 d_a + 26\right)\left(\frac{f'_c}{10}\right)^{0.7} \tag{8}$$

where f'_c is in MPa and d_a is the maximum aggregate size of concrete mix which is taken equal to 10 mm according to test data in [11].

The compressive material properties of the concrete infill require careful consideration. When a CFAT column undergoes axial compression, the concrete infill expands laterally and is confined passively by the aluminium tube resulting in higher strength and ductility of the specimen. Past investigations on CFST [9], demonstrated that after the interaction between the two materials, the concrete infill exhibits triaxial stress state, while the aluminium tube biaxial stress state. In the initial loading stage and up to the peak strength, it is considered that there is no interaction between the two components, as the unequal lateral expansion owing to different Poisson's ratios results in a small gap between the aluminium tube and the concrete infill. Consequently, the ascending part of the stress-strain curve (σ-ε) can be considered identical to that of unconfined concrete. After that, the two materials contact each other, and the specimen yields increased strain at the ultimate strength due to the confining pressure provided to the concrete from the aluminium tube. Upon that state which is represented by a horizontal plateau in the stress-strain diagram, a softening descending branch with increased ductility and less steepness follows. The aforementioned behaviour can be captured by a three-stage stress-strain curve of figure 2 which was proposed for CFST stub columns by Tao et al. [9]. This stress-strain curve is adopted in the current investigation for the modelling of the concrete infill compressive response.

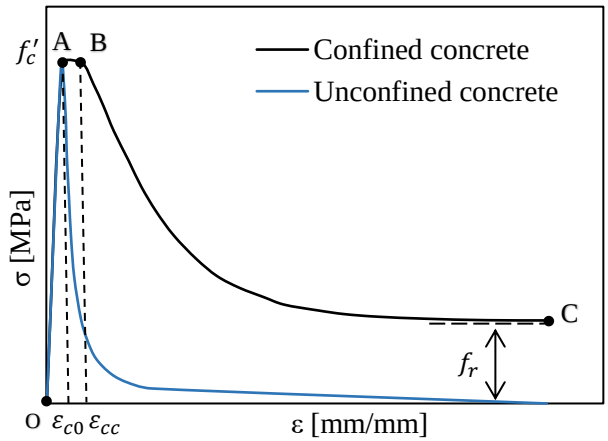

Figure 2. Stress-strain curve for confined concrete suggested by Tao et al. [9].

For the ascending branch (OA), equation (9) proposed by Samani and Attard [8] is used:

$$\frac{\sigma}{f'_c}=\left[\frac{A\cdot X+B\cdot X^2}{1+(A-2)X+(B+1)X^2}\right] \quad for \;\; 0<\varepsilon\le\varepsilon_{c0},\; X=\frac{\varepsilon}{\varepsilon_{c0}};\; A=\frac{\varepsilon_c\varepsilon_{c0}}{f'c};\; B=\frac{(A-1)^2}{0.55}-1 \tag{9}$$

where ε_{c0} is the strain corresponding to the maximum compressive strength of concrete according to equation (10) [24]:

$$\varepsilon_{c0}=0.00076+\sqrt{(0.626\,f'_c-4.33)\cdot 10^{-7}} \tag{10}$$

where f'_c is in MPa.
At point B, the strain ε_{cc} is estimated from equation (11) [8]:

$$\frac{\varepsilon_{cc}}{\varepsilon_{c0}}=\exp\left[(2.9224-0.00367\,f'_c)\left(\frac{f_B}{f'_c}\right)^{0.3124+0.002\,f'_c}\right] \tag{11}$$

where f_B is the confining stress to the concrete provided by the aluminium tube and is determined by equation (12) [9]:

$$f_B=\frac{0.25(1+0.027\,f_y)\exp\left[\left(-0.02\sqrt{h^2+b^2}\right)/t\right]}{1+1.6\exp\left[-10\left(f'_c\right)^{4.8}\right]} \tag{12}$$

where *b* and *h* are the outer width and depth of the aluminium tube respectively.
For the descending branch (BC) of the curve, Tao et al. [9] used an exponential function including the softening fracture energy proposed by Binici [6], as given in equation (13):

$$\sigma = fr + \left(f'_c - f_r \right) \exp\left[-\left(\frac{\varepsilon - \varepsilon_{cc}}{\alpha} \right)^{\beta} \right] \quad for\ \varepsilon \geq \varepsilon_{cc} \tag{13}$$

where f_r is the residual stress as illustrated in figure 2, while the parameters α and β are used to describe the shape of the softening branch. Based on regression analysis [9] for rectangular columns, f_r can be taken equal to f_t and β equal to 0.92, while α can be computed according to equation (14) [9]:

$$\alpha = 0.005 + 0.0075\xi_c, \quad \xi_c = \frac{A_a f_y}{A_c f'_c} \tag{14}$$

where ξ_c is the confinement factor while A_α and A_c are the cross-sectional areas of the aluminium tube and the concrete infill, respectively.
The above parameters calculated for S50.8×50.8×1.6 specimen are listed in table 2.

Table 2. Concrete damage plasticity model parameters calculated for S50.8×50.8×1.6 specimen.

E_c (MPa)	f_{b0}/f'_c	K_c	w_{cr} (mm)	G_F (N/mm)	A	B	ε_{c0} (mm/mm)	ε_{cc} (mm/mm)	f_B (MPa)	α	ξ_c
31590	1.18	0.73	0.10	0.05	2.28	2.0	0.002	0.004	0.90	0.02	1.59

2.6. Modelling of concrete infill-aluminium tube interaction
Surface-to-surface contact was used to model the interaction between the inner surface of the aluminium tube and the outer surface of the concrete infill. “Hard contact” which allows for separation of both surfaces in tension and prevents penetration in compression was employed in the normal direction. The Coulomb friction model was used in the tangential direction. As the loading was implemented simultaneously at both materials there is little or no slip between them and thereby the value of the friction coefficient does not have significant influence on the results. For CFST columns, friction coefficient values of 0.25 [25], 0.3 [26] and 0.6 [27] have been reported. Given that there is limited reported work for CFAT members, a value of 0.3 was used in the current numerical study achieving good convergence with the experimental results (Section 3).

2.7. Analyses
The anticipated failure mode of the CFAT members was flexural buckling, i.e. the sudden loss of stability and deformation at a structured a direction orthogonal to the direction of loading. Structural members subjected to compression (i.e. columns) are prone to buckling phenomena and their ultimate performance can be significantly affected by the presence of initial geometric imperfections. The latter needs to be accurately considered in both experimental and numerical studies. A numerical technique to incorporate these geometric imperfections in the structural members is through an initial execution of an eigenvalue linear buckling analysis. A magnitude of the lowest buckling mode shape corresponding to the experimental failure mode can be introduced in the subsequent analysis, i.e. the nonlinear static analysis. An imperfection magnitude of *L*/1000 where *L* is the length of the members was considered to be good approximation of real structural members and was adopted herein. A non-linear static analysis with Riks method allowing to capture the full-range of the load-deformation path of the FE models was used. The load was imposed on the top of the column in form of displacement, which was similar to the experimental investigation [11]. The effects of the residual stresses were ignored in the current numerical investigation.

3. FE model validation

The accuracy of the developed FE models was validated through comparisons between the experimental [11] and numerical results in terms of the ultimate strengths, load-mid-height lateral displacement curves and failure modes. The experimentally and numerically obtained load-mid-height lateral displacement curves of a typical column specimen are shown in figure 3(a), indicating that the experimental initial stiffness, ultimate capacity and the post-ultimate response can be captured from the developed FE model. The failure modes of the same specimen obtained by test and FEA are illustrated in figure 3(b), showing a very good agreement. The ultimate capacity determined as the maximum load applied during the test (N_{Exp}) and FE (N_{FEA}) are also compared in table 3. The mean value and the corresponding coefficient of variation (COV) of the N_{FEA}/N_{Exp} ratio is 1.00 and 0.084, respectively, demonstrating that the developed FE models can accurately replicate the structural response of CFAT columns under axial compression.

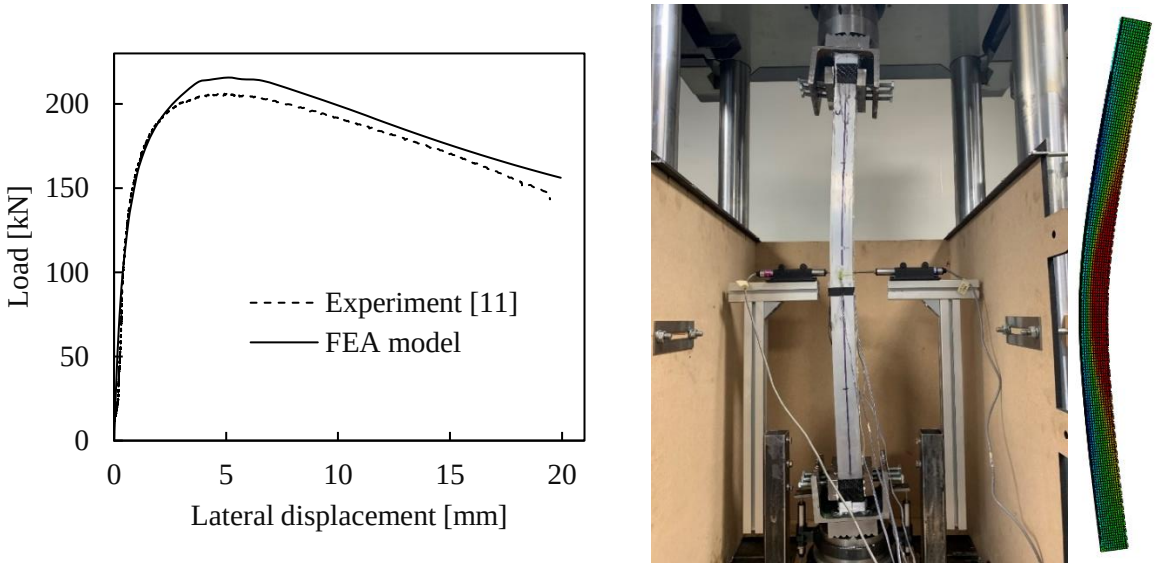

(a) Load-mid height lateral displacement curves (b) Failure mode: flexural buckling

Figure 3. Comparison of experimental [11] and numerical results for R101.6×50.8×3.3 specimen.

Table 3. Comparison of experimental and FEA strengths for CFAT columns.

Specimen	N_{Exp} (kN)	N_{FEA} (kN)	N_{FEA}/N_{Exp}
S50.8×50.8×1.6	103.71	86.29	0.83
S50.8×50.8×3.3	141.18	143.97	1.02
S50.8×50.8×4.8	195.77	175.75	0.90
S76.2×76.2×3.3	344.07	372.09	1.08
S76.2×76.2×4.8	449.68	468.57	1.04
S76.2×76.2×6.4	532.08	564.00	1.06
R76.2×38.1×3.3	107.47	107.47	1.00
R76.2×47.8×3.3	204.27	189.97	0.93
R101.6×25.4×3.3	47.49	52.71	1.11
R101.6×50.8×3.3	206.15	216.46	1.05
Mean value			1.00
COV			0.084

4. Parametric study

Upon the execution of the validation process, a parametric study was performed over a range of cross-sectional aspect ratios (h/b), plate thicknesses for the aluminium tube (t) and characteristic strengths for the concrete infill. The study included one series of SHS with $H \times B$: 50 × 50 and five different plate thicknesses of 1, 2, 3, 4 and 5 mm for the aluminium tubes. The second series comprised of RHS with

$H \times B$: 100 × 50 and five different plate thicknesses of 2, 4, 6, 8 and 10 mm allowing rotation around the minor axis, and the third series same sections with the second series but allowing rotation around the major axis. The selected thicknesses prevented local buckling failure mode. Three different nominal concrete strengths of 30, 50 and 70 MPa were, also, investigated. Average material properties for the aluminium alloy tubes were used as shown in figure 4. The following notation is adopted for their identification: the first part of the notation indicates the type of the section and the number refers to the buckling side of the section in mm, the second part shows the plate thickness of the section in mm and the third part the nominal concrete strength. For example, "R100-2-C30" refers to an RHS under buckling around the major axis (since "100" is the buckling side of the section (100 × 50) which is the bigger one), its plate thickness is equal to 2 mm and the concrete infill is 30 MPa.

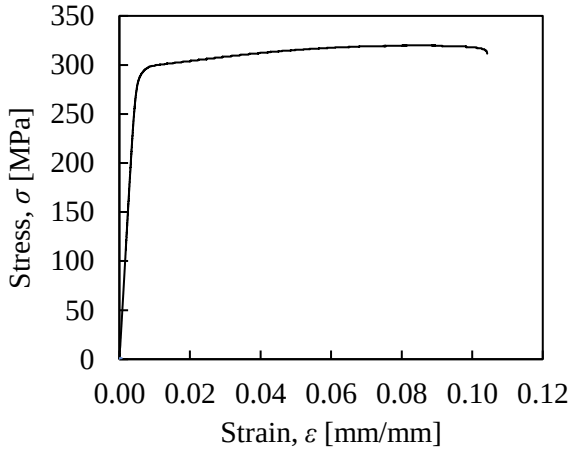

Figure 4. Stress-strain curve employed for aluminium tubes in parametric study.

5. Discussion and design recommendations

The Eurocodes suite consists of 10 European Standards for structural design; Eurocode 9 (EC9) [12] provides design rules for aluminium alloy structures, whilst Eurocode 4 (EC4) [13] for composite steel-concrete structures. In the absence of a codified design provision for aluminium-concrete structures, a combination between EC4 and EC9 is adopted. In particular, the design buckling strength of the CFAT columns was calculated based on the design formulae proposed by EC4 [13], using the aluminium material properties instead of those of steel. The results of the parametric study and the comparison between the concrete-filled aluminium SHS and RHS column strengths obtained from the parametric study (N_{FEA}) and the design strengths ($N_{EC4\text{-}EC9}$) predicted using EC4 in combination with EC9 are presented in Table 4. The mean value and the corresponding coefficient of variation (COV) of the $N_{FEA}/N_{EC4\text{-}EC9}$ ratio is 1.05 and 0.087 respectively. It can be observed that the codified predictions are safe (i.e. the design strength predicted by the European standards are lower than the actual ultimate load capacity), whereas the high COV suggests scattered predictions. It can be concluded that combined European design standards can be utilised to predict the buckling strength of concrete-filled aluminium alloy tubular members. The same conclusions can be drawn from figure 5 where the ultimate strengths obtained by the FE analysis (N_{FEA}) are normalised by the plastic resistance ($N_{pl,Rk}$) and plotted against the normalised slenderness λ (i.e. a measure of the propensity of a column to buckling), calculated according to [12]. The Eurocode design column strength curve is also included in the same figure. The fact that the FEA results are above the EC4-EC9 curve suggests again safe predictions, but with an apparent scatter, with respect to accuracy (i.e. distance from EC4-EC9 design curve).

Finally, figures 6(a)-(c) depict the relationship between the column strengths determined by FEA and design rules for the investigated nominal concrete strengths. As anticipated, the column buckling resistance increases as the concrete strength grade becomes higher and as the aluminium wall thickness increases.

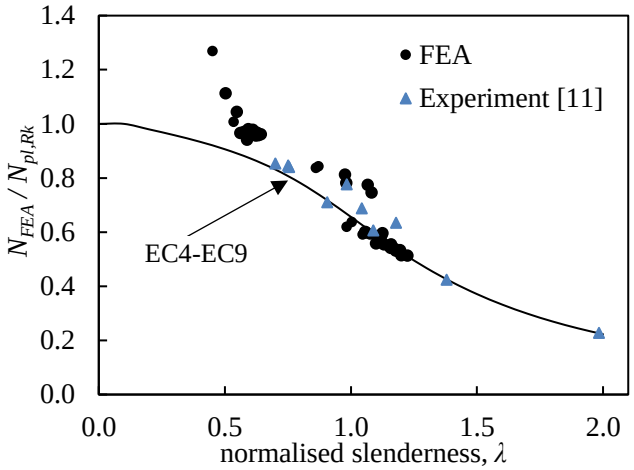

Figure 5. Comparison between normalised ultimate loads and normalised slenderness of CFAT columns.

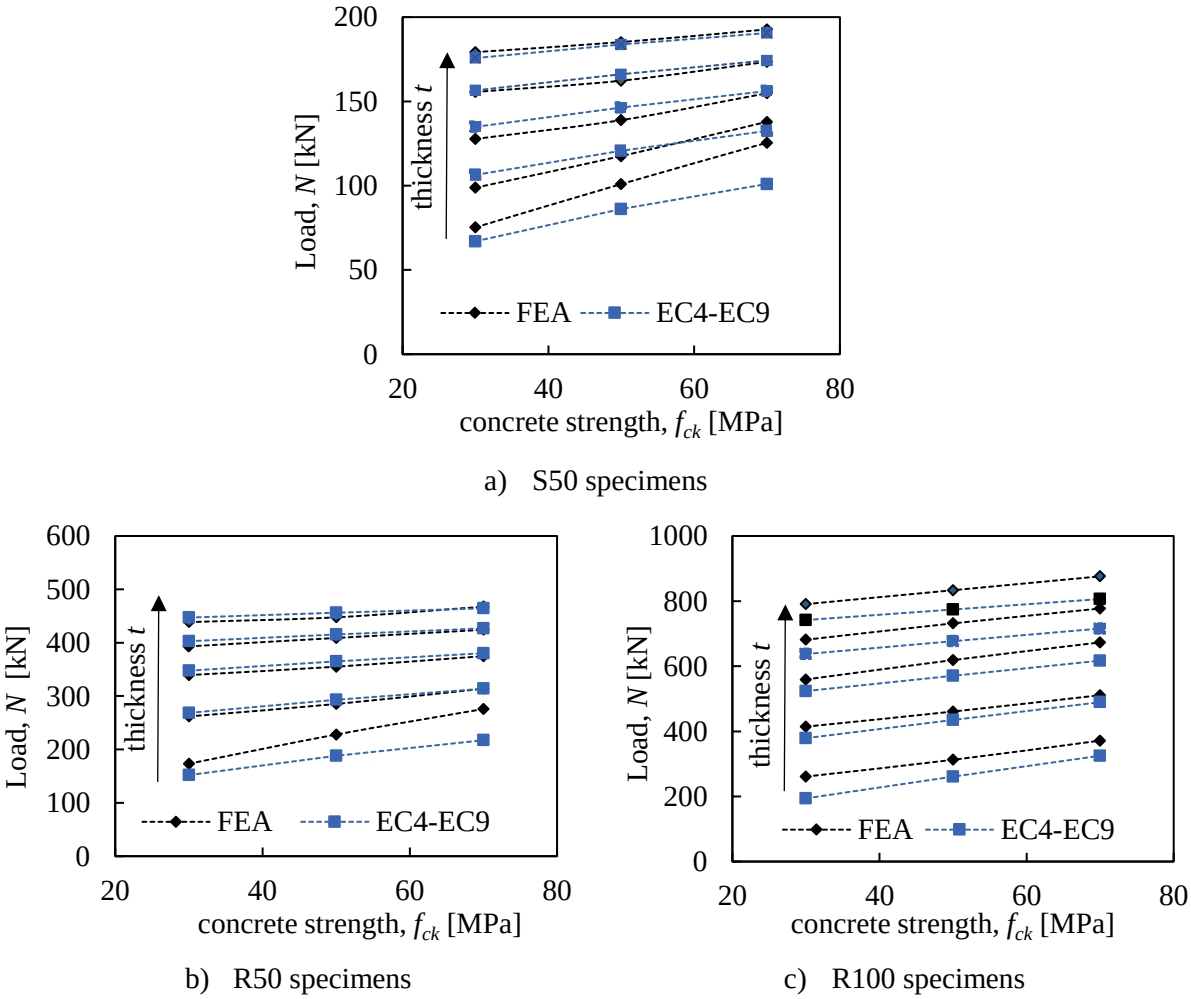

a) S50 specimens

b) R50 specimens

c) R100 specimens

Figure 6. Results of parametric study together with EC4-EC9 predictions.

Table 4. Properties and results of the parametric study.

Specimen	Height, h (mm)	Width, b (mm)	h/b	Thickness, t (mm)	Length, L (mm)	f_{ck} (MPa)	N_{FEA} (kN)	$N_{EC4\text{-}EC9}$ (kN)	N_{FEA} / $N_{EC4\text{-}EC9}$
S50-1-C30	50	50	1	1	1000	30	75.26	67.00	1.12
S50-2-C30	50	50	1	2	1000	30	98.80	106.40	0.93
S50-3-C30	50	50	1	3	1000	30	127.72	134.87	0.95
S50-4-C30	50	50	1	4	1000	30	155.63	156.54	0.99
S50-5-C30	50	50	1	5	1000	30	179.22	175.70	1.02
S50-1-C50	50	50	1	1	1000	50	100.94	86.17	1.17
S50-2-C50	50	50	1	2	1000	50	117.55	120.73	0.97
S50-3-C50	50	50	1	3	1000	50	138.89	146.42	0.95
S50-4-C50	50	50	1	4	1000	50	162.28	166.13	0.98
S50-5-C50	50	50	1	5	1000	50	185.17	183.67	1.01
S50-1-C70	50	50	1	1	1000	70	125.50	101.00	1.24
S50-2-C70	50	50	1	2	1000	70	137.88	132.49	1.04
S50-3-C70	50	50	1	3	1000	70	154.84	156.14	0.99
S50-4-C70	50	50	1	4	1000	70	173.48	174.32	1.00
S50-5-C70	50	50	1	5	1000	70	192.71	190.54	1.01
R50-2-C30	100	50	2	2	1000	30	173.32	151.94	1.14
R50-4-C30	100	50	2	4	1000	30	261.95	268.55	0.98
R50-6-C30	100	50	2	6	1000	30	339.37	347.54	0.98
R50-8-C30	100	50	2	8	1000	30	393.12	402.81	0.98
R50-10-C30	100	50	2	10	1000	30	438.64	447.11	0.98
R50-2-C50	100	50	2	2	1000	50	227.94	188.38	1.21
R50-4-C50	100	50	2	4	1000	50	285.17	293.15	0.97
R50-6-C50	100	50	2	6	1000	50	355.04	365.16	0.97
R50-8-C50	100	50	2	8	1000	50	408.92	415.65	0.98
R50-10-C50	100	50	2	10	1000	50	447.59	456.25	0.98
R50-2-C70	100	50	2	2	1000	70	275.76	217.23	1.27
R50-4-C70	100	50	2	4	1000	70	313.82	313.82	1.00
R50-6-C70	100	50	2	6	1000	70	374.86	380.34	0.99
R50-8-C70	100	50	2	8	1000	70	424.22	426.90	0.99
R50-10-C70	100	50	2	10	1000	70	467.52	464.37	1.01
R100-2-C30	100	50	2	2	1000	30	261.02	194.14	1.34
R100-4-C30	100	50	2	4	1000	30	414.30	379.04	1.09
R100-6-C30	100	50	2	6	1000	30	559.34	523.69	1.07
R100-8-C30	100	50	2	8	1000	30	681.39	637.44	1.07
R100-10-C30	100	50	2	10	1000	30	790.79	741.81	1.07
R100-2-C50	100	50	2	2	1000	50	312.53	260.59	1.20
R100-4-C50	100	50	2	4	1000	50	460.72	434.96	1.06
R100-6-C50	100	50	2	6	1000	50	618.90	570.87	1.08
R100-8-C50	100	50	2	8	1000	50	731.55	676.97	1.08
R100-10-C50	100	50	2	10	1000	50	833.48	774.41	1.08
R100-2-C70	100	50	2	2	1000	70	371.45	325.10	1.14
R100-4-C70	100	50	2	4	1000	70	510.94	489.53	1.04
R100-6-C70	100	50	2	6	1000	70	673.07	617.00	1.09
R100-8-C70	100	50	2	8	1000	70	777.26	715.68	1.09
R100-10-C70	100	50	2	10	1000	70	876.05	806.36	1.09
								Mean value	1.05
								COV	0.087

6. Conclusions

The current study investigated numerically the structural response of concrete-filled aluminium SHS and RHS members under axial compressive loading. The stress-strain relationship of the confined concrete has been considered within the simulations. Material non-linearities and geometric imperfections were, also, included. The accuracy of the developed FE model was evaluated on the basis of available test results, in terms of the initial stiffness, the maximum load-bearing capacity and the failure pattern. An extensive parametric study was subsequently conducted. The column strengths obtained from the parametric study were compared with the design strengths predicted by the European standards, i.e. EC4 in combination with EC9. The results demonstrate that the existing design criteria are able to generally provide safe predictions. Further experimental and numerical investigation is needed to obtain a clear perspective of the structural behaviour of CFAT columns, aiming to properly modify the existing design specifications and achieve more accurate provisions.

Acknowledgments

The financial support of the Faculty of Engineering and Technology of Liverpool John Moores University is gratefully acknowledged.

References

[1] Georgantzia E, Gkantou M and Kamaris GS 2021 Aluminium alloys as structural material: A review of research *Eng. Struct*. 227. 111372
[2] Zhou F and Young B 2008 Tests of concrete-filled aluminum stub columns *Thin-Walled Struct*. **46**(6) 573-83
[3] Zhou F and Young B 2009 Concrete-filled aluminum circular hollow section column tests *Thin-Walled Struct.* **47**(11) 1272-80
[4] Zhou F and Young B 2012 Numerical analysis and design of concrete-filled aluminum circular hollow section columns *Thin-Walled Struct.* **50**(1) 45-55
[5] Zhou F and Young B 2018 Concrete-filled double-skin aluminum circular hollow section stub columns *Thin-Walled Struct.* **133** 141-52
[6] Binici B 2005 An analytical model for stress-strain behavior of confined concrete. *Eng Struct.* **27**(7) 1040-51
[7] Ellobody E and Young B 2006 Nonlinear analysis of concrete-filled steel SHS and RHS columns *Thin-Walled Struct.* **44**(8) 919-30
[8] Samani AK and Attard MM 2012 A stress-strain model for uniaxial and confined concrete under compression *Eng Struct.* **41** 335-49
[9] Tao Z, Wang Z Bin and Yu Q 2013 Finite element modelling of concrete-filled steel stub columns under axial compression *J Constr Steel Res.* **89** 121-31
[10] ABAQUS. 2018 ABAQUS Standard User's Manual. Version 6.14. Providence. RI (USA): Dassault Systemes Corp.
[11] Georgantzia E, Bin Ali S, Gkantou M, Kamaris GS, Kansara K and Atherton W 2021 Structural response of aluminium alloy concrete filled tubular columns *Proc. of Eurosteel (Sheffield/United Kingdom)*
[12] European Committee for Standarization (EC9) 2007 *Eurocode 9 : Design of aluminium structures. Part 1-1: General structural rules - General structural rules and rules for buildings* BS EN 1999-1-1:2007. CEN:2007
[13] European Committee for Standardisation (EC4) 2004 *Eurocode 4: Design of Composite Steel and Concrete Structures. Part 1-1: General Rules and Rules for Buildings* BS EN 1994-1-1: 2004. CEN:2004.
[14] Tziavos NI, Gkantou M, Theofanous M, Dirar S and Baniotopoulos C (2020) Behaviour of grout-filled double-skin tubular steel stub-columns: Numerical modelling and design considerations. In *Structures.* **27** 1623-1636

[15] Gkantou M, Theofanous M and Baniotopoulos C (2020) A numerical study of prestressed high strength steel tubular members *Frontiers of Structural and Civil Engineering.* **14**(1)10-22.
[16] Bin Ali S, Kamaris G S, Gkantou M, Kansara K and Hashim K (2020) Numerical study of concrete-filled aluminium alloy tubular columns under eccentric compression. In *IOP Conference Series: Materials Science and Engineering.* IOP Publishing (Accepted)
[17] European Committee for Standardisation (EC2) 2004 *Eurocode 2: Design of Concrete Structures. Part 1-1: General rules and rules for buildings* BS EN 1992-1-1: CEN:2004.
[18] Papanikolaou VK and Kappos AJ 2007 Confinement-sensitive plasticity constitutive model for concrete in triaxial compression *Int J Solids Struct.* **44**(21) 7021-48
[19] Yu T, Teng JG, Wong YL and Dong SL 2010 Finite element modeling of confined concrete-I: Drucker-Prager type plasticity model. *Eng Struct.* **32**(3) 665-79
[20] Hillerborg A, Modéer M and Petersson PE 1976 Analysis of crack formation and crack growth in concrete by means of fracture mechanics and finite elements *Cem Concr Res.* **6**(6) 773-81
[21] Hordijk DA 1991 *Local approach to fatigue of concrete* Ph.D. thesis (Delft Univ. of Technology/Delft/Netherlands)
[22] CEB-FIP Model Code 1990 (London: Thomas Telford Ltd)
[23] Bažant ZP and Becq-Giraudon E 2002 Statistical prediction of fracture parameters of concrete and implications for choice of testing standard *Cem Concr Res.* **32**(4) 529-56
[24] De Nicolo B, Pani L and Pozzo E 1994 Strain of concrete at peak compressive stress for a wide range of compressive strengths *Mater Struct.* **27**(4) 206-10
[25] Schneider SP 1998 Axially loaded concrete-filled steel tubes *J Struct Eng.* **124**(10) 1125-38
[26] Lam D, Dai XH, Han LH, Ren QX and Li W 2012 Behaviour of inclined, tapered and STS square CFST stub columns subjected to axial load *Thin-Walled Struct.* **54** 94-105
[27] Han LH, Yao GH and Tao Z 2007 Performance of concrete-filled thin-walled steel tubes under pure torsion *Thin-Walled Struct.* **45**(1) 24-36